Translational Science

Cancer Research

LRRC15 Is a Novel Mesenchymal Protein and Stromal Target for Antibody–Drug Conjugates

James W. Purcell[1], Sonia G. Tanlimco[1], Jonathan Hickson[2], Melvin Fox[1], Mien Sho[1], Lisa Durkin[3], Tamar Uziel[2], Rick Powers[1], Kelly Foster[2], Thomas McGonigal[2], Subashri Kumar[1], Josue Samayoa[1], Dong Zhang[1], Joann P. Palma[2], Sasmita Mishra[2], Diane Hollenbaugh[1], Kurt Gish[1], Susan E. Morgan-Lappe[2], Eric D. Hsi[3], and Debra T. Chao[1]

Abstract

Progress in understanding tumor stromal biology has been constrained in part because cancer-associated fibroblasts (CAF) are a heterogeneous population with limited cell-type–specific protein markers. Using RNA expression profiling, we identified the membrane protein leucine-rich repeat containing 15 (LRRC15) as highly expressed in multiple solid tumor indications with limited normal tissue expression. LRRC15 was expressed on stromal fibroblasts in many solid tumors (e.g., breast, head and neck, lung, pancreatic) as well as directly on a subset of cancer cells of mesenchymal origin (e.g., sarcoma, melanoma, glioblastoma). LRRC15 expression was induced by TGFβ on activated fibroblasts (αSMA^+) and on mesenchymal stem cells. These collective findings suggested LRRC15 as a novel CAF and mesenchymal marker with utility as a therapeutic target for the treatment of cancers with LRRC15-positive stromal desmoplasia or cancers of mesenchymal origin. ABBV-085 is a monomethyl auristatin E (MMAE)-containing antibody–drug conjugate (ADC) directed against LRRC15, and it demonstrated robust preclinical efficacy against LRRC15 stromal-positive/cancer-negative, and LRRC15 cancer-positive models as a monotherapy, or in combination with standard-of-care therapies. ABBV-085's unique mechanism of action relied upon the cell-permeable properties of MMAE to preferentially kill cancer cells over LRRC15-positive CAF while also increasing immune infiltrate (e.g., $F4/80^+$ macrophages) in the tumor microenvironment. In summary, these findings validate LRRC15 as a novel therapeutic target in multiple solid tumor indications and support the ongoing clinical development of the LRRC15-targeted ADC ABBV-085.

Significance: These findings identify LRRC15 as a new marker of cancer-associated fibroblasts and cancers of mesenchymal origin and provide preclinical evidence for the efficacy of an antibody-drug conjugate targeting the tumor stroma. *Cancer Res; 78(14); 4059–72. ©2018 AACR.*

Introduction

Many cancer types with high stromal content, such as pancreatic cancer, triple-negative breast cancer, non–small cell lung cancer (NSCLC) and sarcoma, continue to have low response rates to current therapies and poor long-term survival (1–3). It has been proposed that extracellular matrix (ECM) proteins generated by cancer-associated fibroblasts (CAF) found in tumor stroma impede the effective uptake of traditional chemotherapeutics, and contribute to the immunosuppressive environment seen in most solid tumors (4–7). Disrupting the ECM to improve drug delivery is a strategy that is being pursued preclinically as well as in early clinical trials in stroma-rich tumors such as pancreatic cancer (8–10).

CAFs are a heterogeneous cell population with high degrees of cellular plasticity, which are thought to arise from numerous cell types including resident fibroblasts, endothelial cells, cells undergoing epithelial-to-mesenchymal transition (EMT), and mesenchymal stem cells (MSC; refs. 11, 12). This is a rapidly evolving area of tumor biology, with many outstanding questions still remaining regarding the origin, prevalence, and biological function of these CAF populations across different tumor types. Fibroblasts in the tumor microenvironment (TME) are typically characterized by expression of proteins such as α-smooth muscle actin (α-SMA) or fibroblast activation protein alpha (FAPα), both of which have significant normal tissue expression, leading researchers in this field to emphasize the need for additional CAF markers that are more TME specific (13–15).

In this study, we characterize leucine-rich repeat containing 15 (LRRC15), a 581 amino acid type I membrane protein with no obvious intracellular signaling domains, which was found to be highly expressed on the cell surface of stromal fibroblasts in many solid tumors. In this manuscript, we describe the first detailed evaluation of the expression of LRRC15 on cancer and normal tissues.

Attaching a cytotoxic payload onto a cancer-targeting antibody to generate an antibody–drug conjugate (ADC) is a therapeutic strategy used to deliver cytotoxic molecules to cancer cells and elicit an antitumor response (16, 17). The high LRRC15 expression we observed in multiple solid tumor indications together with its low normal tissue expression led us to evaluate the utility of LRRC15 as a targeting antigen to deliver a growth-inhibitory

[1]AbbVie Biotherapeutics, Redwood City, California. [2]AbbVie Inc., North Chicago, Illinois. [3]Cleveland Clinic, Cleveland, Ohio.

Note: Supplementary data for this article are available at Cancer Research Online (http://cancerres.aacrjournals.org/).

J.W. Purcell and S.G. Tanlimco contributed equally to this work.

Corresponding Author: James W. Purcell, AbbVie Biotherapeutics, 1500 Seaport Boulevard, Redwood City, CA 94063. Phone: 415-430-8566; E-mail: james.purcell@abbvie.com

doi: 10.1158/0008-5472.CAN-18-0327

payload to the TME in the form of an ADC. ABBV-085 is an ADC composed of an anti-LRRC15 humanized IgG1 antibody (Ab1), conjugated to the antimitotic drug monomethyl auristatin E (MMAE) via a protease cleavable valine–citrulline (vc) linker. This novel stromal-targeting ADC is currently being evaluated in a phase I first-in-human safety study.

Materials and Methods

Antibodies, drug conjugates, and proteins

Multiple anti-LRRC15 antibodies with different characteristics were generated: (i) Ab1/Ab2-humanized IgG1 kappa antibodies that bind human, cyno, rat, and mouse extracellular LRRC15; (ii) Ab3/Ab4-murine IgG2a antibodies that bind human, cyno, rat, and mouse extracellular LRRC15; and (iii) Ab5-murine IgG2b that binds human extracellular LRRC15 and is formalin fixed paraffin embedded (FFPE) compatible.

ABBV-085, a humanized anti-LRRC15 ADC, contains hydrophobic interaction chromatography (HIC)-enriched E2, where approximately two vcMMAE drugs are conjugated per antibody (Ab1). ADCs with varying drug antibody ratios (mixture of 0, 2, 4, 6, 8 drugs per mAb) were generated as comparison materials to ABBV-085, using published techniques (18). Anti-LRRC15-mcMMAF (E2) was generated with Ab1 conjugated via a non-cleavable maleimido-caproyl linker to form a broad ADC distribution (0, 2, 4, 6, 8 MMAFs per mAb) and subsequently HIC-enriched to contain approximately two molecules of MMAF conjugated to each antibody. An isotype antibody against tetanus toxoid, and isotype ADCs, were used as controls.

The LRRC15 protein used to characterize antibody binding consisted of: extracellular domain (ECD aa22–526) LRRC15-Fc fusion. Recombinant human TGFβ (rhTGFβ1; R&D Systems) was reconstituted at 20 μg/mL in sterile 4 mmol/L HCL with 1 mg/mL BSA, and used at 10 ng/mL unless otherwise stated.

Compounds and formulation

All antibodies and ADCs were formulated in 15 mmol/L histidine, 7% (w/v) sucrose, 0.03% polysorbate 80, pH 6.0, and stored at −80°C. Antibodies and ADCs were diluted in PBS or 15 mmol/L histidine pH 6 prior to administration. A mouse IgG2a anti-PD1 mAb (17D2) was generated in-house and formulated in PBS. Gemcitabine was obtained from Hospira and formulated in 0.9% NaCl. Erlotinib was obtained from OSI Pharmaceuticals and formulated in 2% (vol) DMSO, 98% vol of: 2% (vol) EtOH + 5% (vol) Tween-80 + 20% (vol) PEG-400 + 71% (vol) HPMC. Cetuximab was obtained from Imclone Systems Inc., and formulated in 15 mmol/L histidine buffer, pH 6. Carboplatin was obtained from Hospira, Inc., and formulated in PBS. Docetaxel was obtained from Sagent and formulated in 0.9% NaCl. Radiation treatment was administered to the tumor using a cesium-137 biological irradiation system (Precision X-Ray) with the remainder of the body shielded from the source.

Cell culture

U118-MG (ATCC), PANC-1 (ATCC) were grown in DMEM. RPMI7951 cells (ATCC) were grown in Eagle's Minimum Essential Medium. HCT116 (ATCC) and HCT116-LRRC15 transfectant (with G418 selection, 500 μg/mL) were cultured in McCoy media. Normal human lung fibroblast (NHLF; Lonza), EBC-1 (JCRB), and all additional cells were grown in RPMI1640 media. Unless otherwise noted, all cell lines were supplemented with 10% FBS and cultured at 37°C with 5% CO_2. The identity of cell lines was confirmed according to ATCC recommended guidelines (DNA fingerprinting) and maintained at low passage numbers (<10) and routinely tested for mycoplasma (MycoFluor ThermoFisher).

Human bone marrow–derived MSCs (BM-MSC) that were positive for CD29, CD44, CD73, CD90, CD105, CD166, negative for CD14, CD34, CD45 were purchased from ATCC, and Lonza and grown in vendor recommended media. Adipose-derived MSCs (ATCC) and umbilical cord-derived MSCs (ATCC) were grown in vendor's recommended low serum formulation. BALB/c mouse MSCs (Cyagen) were grown in vendor-specific recommended media under normoxic conditions.

Immunohistochemistry

Normal or cancer human tissues in FFPE blocks or unstained slides were purchased from various commercial vendors (Zion, Asterand, ClinPath Advisors, or US Biomax) for LRRC15 staining performed at AbbVie. All the tissues stained at Dr. Eric Hsi's laboratory were from the tissue bank at Cleveland Clinic Foundation (CCF). All human samples were deidentified to be in compliance with the CCF and AbbVie institutional and corporate policies.

For human LRRC15 staining, FFPE slides were air dried at room temperature. Antigen retrieval was performed with high pH target retrieval buffer at 125°C for 1 minute. Slides were incubated with an AbbVie internally generated human-specific LRRC15 antibody (Ab5, mouse IgG2b) at 1 μg/mL for 60 minutes after protein blocking, followed by HRP mEnvision reagent for 30 minutes and visualized with DAB reaction. Alexa Fluor 488/Alexa Fluor 594 secondary antibody reagents (Thermo Fisher) were used for the immunofluorescence dual staining for LRRC15 and αSMA (clone 1A4; DAKO).

For LRRC15 staining in mouse tissues, optimal cutting temperature (OCT) embedded frozen blocks were sectioned and fixed in acetone before staining with biotinylated mouse anti-mouse LRRC15 antibody (Ab3, mouse IgG2a) at 2 μg/mL after protein block. The antibody-specific binding was detected with ABC-Elite HRP and DAB reaction (DAKO mouse Envision +). LRRC15 expression in xenograft and patient-derived xenograft (PDX) tumors was scored qualitatively from 0 to 3+ based on intensity and frequency of the staining. Other antibodies used for IHC were purchased from commercial vendors including anti-phospho-histone H3 (pHH3) at serine 10, anti-Ki67, anti-CD45 (Cell Signaling Technology) and anti-F4/80 (eBioscience).

Whole section images were scanned with the Aperio Scanscope XT. The percent of positive tumor cells for the mitosis marker (pHH3) in viable tumor areas of whole section images were quantitatively analyzed using a color deconvolution algorithm (Spectrum Image Analysis Program; Aperio).

Immunoblotting

Lysates were quantitated using Pierce BCA Protein Assay Kit. Fifteen micrograms of protein was loaded on a 4% to 12% Bis Tris Gel with 3-(N-morpholino)propanesulfonic acid (MOPS) running buffer and transferred to a polyvinylidene difluoride (PVDF) membrane (Bio-Rad Transblot Turbo). Anti-LRRC15 (Ab5) was used at 0.5 μg/mL, anti-αSMA (DAKO; Clone 1A4) at 1:500, anti-GAPDH (Santa Cruz Biotechnology) at 1:1,000, and goat anti-mouse IgG HRP (Jackson Labs) at 1:10,000.

Flow cytometry

LRRC15 expression was assessed by flow cytometry using either Ab1 and Goat F(Ab')2 antihuman IgG Fc gamma RPE (Jackson ImmunoResearch) secondary, or using AF647-conjugated anti-LRRC15 Ab1 or Ab2. A humanized IgG1 anti-tetanus toxoid antibody with and without fluor labeling was used as an irrelevant isotype control. LRRC15 cell surface copy number was performed using LRRC15 Ab3 (AF488 labeled) relative to isotype-AF488 and quantification was determined with Quantum Simply Cellular Bead Kit (Polysciences) according to the manufacturer's guidelines.

For cell-cycle analysis, trypsinized cells were pelleted and fixed for 30 minutes with ice-cold 85% ethanol (5 mL). The cells were centrifuged out of the ethanol and resuspended in 1 mL of PBS to rehydrate. The cells were centrifuged again and resuspended in 1 mL of 1× propidium iodide, 1× RNAase A and incubated for 1 hour at 37°C and then analyzed by flow cytometry.

For *ex vivo* flow cytometry of dissociated tumors, tumor tissues were minced with scissors and dissociated into single-cell suspensions using the MACS Human Tumor Dissociation Kit (Miltenyi Biotec) per the manufacturer's protocol for the dissociation of tough tumors. Briefly, this involved two, 30 minute, 37°C, enzymatic digestion steps and two mechanical disruption pulses using the gentleMACS C Tube on a gentleMACS Dissociator. Dissociated tumor cells were passed through a 70-μm filter, and immediately used for flow cytometry. Single-cell suspensions were resuspended in PBS with 10% FBS and 10 μg/mL FcR block (antimouse CD16/CD32, clone 93; eBioscience). The following directly conjugated antibodies were used for flow cytometry: human IgG1 κ isotype control AF647, anti-LRRC15 (Ab2)-AF647, anti-FAP-AF647, mouse antihuman CD326 (EpCAM) PE (clone 1B7; eBioscience) and anti-mouse F4/80 PE (clone BM9; eBioscience). *Ex vivo* tumor suspensions were incubated with fluor-conjugated antibodies for 20 minutes on ice and washed twice using PBS with 1% FBS. Flow cytometry data were collected on either a Becton Dickinson FACSCalibur or LSR Fortessa flow cytometer and analyzed using either CellQuest (Becton Dickinson) or FlowJo analysis software (Treestar).

siRNA knockdown

siRNA oligonucleotides for nontargeting control pool/single and LRRC15 ($n = 4$ oligos) were purchased from Dharmacon and resuspended to form 20 μmol/L stock according to the manufacturer's guidelines. Cells were seeded at 5×10^5 cells per well in six-well plates and transfected with 30 pmol of siRNA using Lipofectamine RNAiMax (Thermo Fisher) and Opti-MEM media according to the manufacturer's instructions. Cells were analyzed by flow cytometry for LRRC15 expression 48 hours after transfection with siRNA.

Cell proliferation assay

Inhibition of proliferation was assessed in 96-well format using CellTiterGlo (Promega) after 4 days of treatment with a titration series of specified compounds. Luminescence (measuring ATP) was read on a Perkin Elmer 2030 Victor X5 plate reader. Cell viability was expressed as a percentage relative to untreated control.

Animal husbandry

All mice strains used for efficacy studies, as well as male/female Sprague Dawley rats used in tolerability studies, were obtained from Charles River. Food and water were available *ad libitum*. Mice/rats were acclimated to the animal facilities for a period of at least 1 week prior to commencement of experiments. Animals were tested in the light phase of a 12-hour light:12-hour dark schedule. All *in vivo* experiments were reviewed, approved, and conducted in compliance with AbbVie's Institutional Animal Care and Use Committee and the NIH Guide for Care and Use of Laboratory Animals guidelines in a facility accredited by the Association for the Assessment and Accreditation of Laboratory Animal Care.

Mouse xenograft efficacy

The following mice strains (all female) were used for efficacy studies, C57BL/6 (MC38), CB17-SCID (EBC1, U118MG, SUM190PT, SCC15, PANC1), SCID-Beige (NCI-H1650), and NSG (osteosarcoma CTG-0241). For each xenograft study, 5 to 10 million viable cells (injection volume 0.1 mL) were inoculated subcutaneously into the right flank of mice. Cells were implanted with matrigel (1:1 mixture of S-MEM and Matrigel), unless otherwise stated. Tumors were randomized and size matched for initiation of treatment in efficacy studies once tumor volumes grew to 150 to 200 mm^3. Mice weighed approximately 20 g at the onset of therapy. Tumor volume was estimated two times weekly. Measurements of the length (L) and width (W) of the tumor were taken via electronic caliper and the volume was calculated according to the following equation: $V = (L \times W^2)/2$. Mice were euthanized when tumor volume reached 2,000 mm^3 or if skin ulcerations occurred.

Tumor growth inhibition (TGI) indicates the divergence between the mean tumor volume of a drug-treated group and the mean tumor volume of the control-treated group and is expressed as a percentage of the mean volume of the control group. TGI_{max} (maximum TGI = 100 × [1 − (mean tumor volume of treatment group/mean tumor volume of control group)] was determined at the time point when difference between treatment and control groups was maximal ($N = 8$ mice per group). Values for rate of complete response (CR) is given as the percentage of mice within a group with a tumor burden $\leq$25 mm^3 for at least three consecutive measurements. Partial response (PR) is given as the percentage of mice within a group with tumor burden less than half of their starting tumor volume at time of randomization but >25 mm^3 for three consecutive measurements. Data calculations were made and stored using Study Log, Study director Version 2.1.

Statistical analysis

Data from experiments *in vivo* were analyzed using the two-way ANOVA with *post hoc* Bonferroni correction for T/C values (JMP Version 10.0.0; SAS Institute Inc.), and the Mantel–Cox log-rank test for TGD (JMP Version 10.0.0; SAS Institute Inc.). Statistical analysis for determining significance between treatment groups for *in vitro* experiments was performed using two-tailed T tests in GraphPad Prism.

Results

LRRC15 is highly expressed in tumor stroma and on cancer cells of mesenchymal origin

RNA expression analysis of over 2,000 distinct cancer patient samples representing multiple indications and 350 normal human tissues was undertaken to identify antigens differentially expressed between cancer and normal tissues. From this

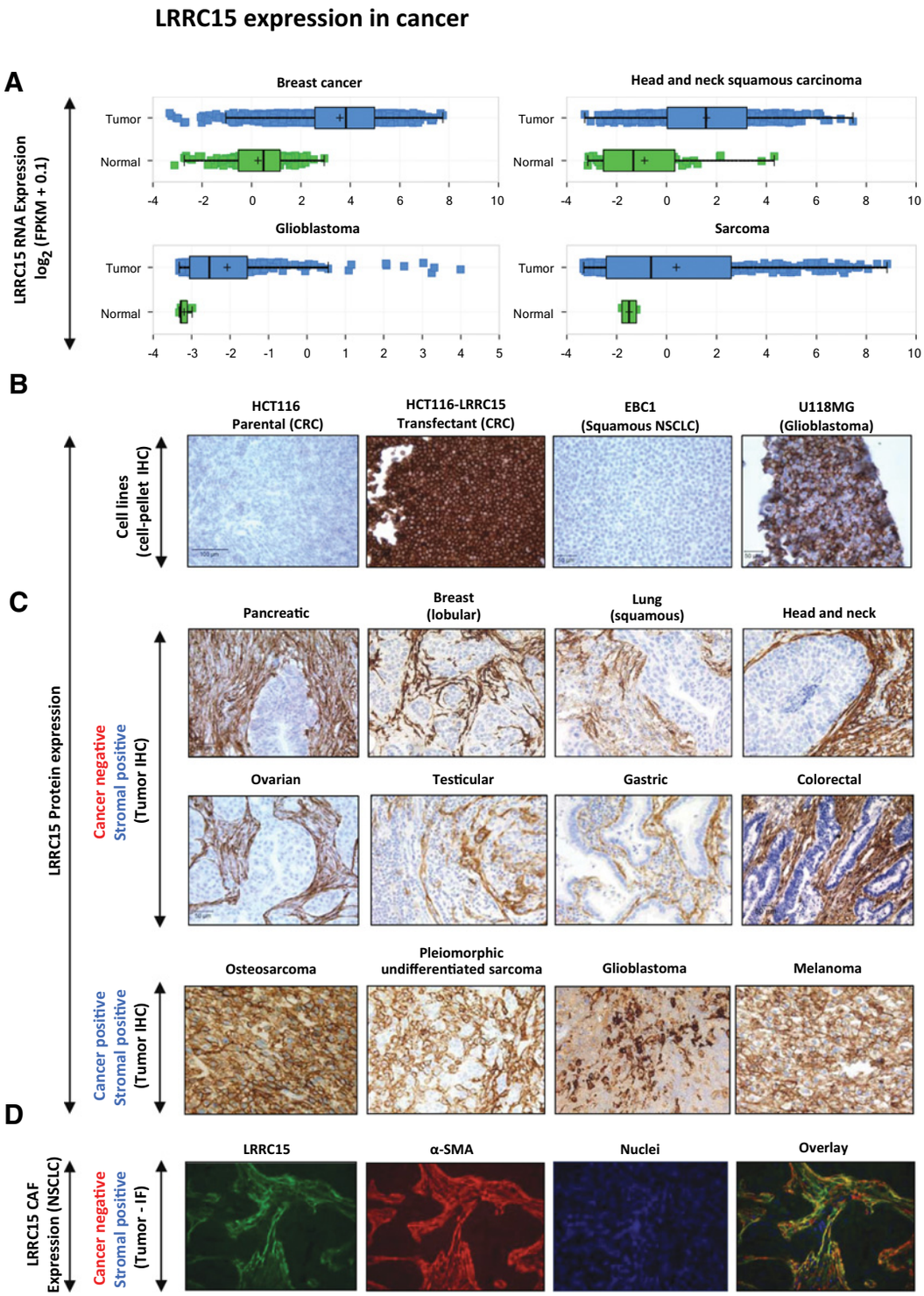

Figure 1.

LRRC15 expression in cancer. **A,** RNA-seq data from TCGA analyzed using ArrayStudio software (OmicSoft, http://www.omicsoft.com) showing LRRC15 RNA expression on multiple solid tumor indications relative to the normal tissue of origin. Axis units are Log_2 (FPKM + 0.1). **B,** LRRC15-negative cell line HCT116 and HCT116 cells stably expressing LRRC15 were cultured *in vitro*, pelleted, and made as FFPE blocks for LRRC15 IHC. LRRC15-negative cell line EBC-1 and LRRC15-positive cell line U118MG are shown for comparison. **C,** Representative IHC analysis of LRRC15 expression (brown) in solid tumors, where expression is cancer-negative and stromal-positive (top) or cancer-positive and stromal-positive (bottom). **D,** Fluoresencent IHC of LRRC15 (green) colocalization with activated fibroblast marker (α-SMA, red) in a representative example of NSCLC (adenocarcinoma). Nuclei of cells are stained with DAPI (blue). IF, immunofluorescence.

analysis, LRRC15 was identified as having high expression and prevalence across multiple solid tumors, with low expression in most normal tissues. Publically available data from The Cancer Genome Atlas (TCGA, https://cancergenome.nih.gov/) confirmed this finding (Fig. 1A; Supplementary Fig. S1), and is consistent with published reports of LRRC15 overexpression in breast cancer (19, 20).

To confirm RNA expression findings, we examined LRRC15 protein expression in cancer and normal tissues by IHC. Multiple commercially available antibodies to LRRC15 were found to be lacking specificity, leading us to generate new highly selective antibodies to the extracellular domain of LRRC15. The specificity of our LRRC15 antibodies was extensively tested on LRRC15 recombinant protein, LRRC15-positive (e.g., U118MG) and -negative (e.g., HCT116, EBC1) endogenous cell lines, and on LRRC15-transfectant cells compared with the negative parental cell line (HCT-116). LRRC15 immunofluorescence and IHC performed on cell pellets (Fig. 1B; Supplementary Fig. S2A, S2B) corresponds with flow cytometry protein expression data (Supplementary Fig. S2C). In addition, we show that commercially acquired siRNA oligonucleotides ($n = 4$) to LRRC15 resulted in loss of expression and loss of antibody binding 48 hours post-siRNA transfection (Supplementary Fig. S2D).

The prevalence of LRRC15 protein expression across tumor types by IHC was found to be highly concordant with that observed by mRNA expression analysis. Interestingly, rather than being expressed by the cancer cells, LRRC15 was predominantly expressed at high levels on the stromal cells in the TME (Fig. 1C; Table 1). Tumor stromal IHC expression of LRRC15 ($\geq$2+, 25%) was detected across a diverse set of solid tumor cancer types. High LRRC15 prevalence was seen for multiple cancer indications including breast cancer (94%, $n = 82/87$ representing all subtypes), head and neck (81%, $n = 182/226$), NCSLC (72% adeno, $n = 63/87$ and 64% squamous, $n = 74/115$), and pancreatic (66%, $n = 27/41$). Conversely, there were certain indications that had negligible or no LRRC15 expression such as renal cancer (3%, $n = 1/31$), prostate (0%, $n = 0/34$), and GIST (0%, $n = 0/6$). We also observed stromal LRRC15 expression in metastases from various sites (lymph node, bone, liver). LRRC15 stromal positivity is shown in a matched primary head and neck tumor (tongue) and lymph node metastasis from the same patient (Supplementary Fig. S2E). Specific noncarcinoma cancers with mesenchymal characteristics were identified as having both cancer and stromal expression of LRRC15, including sarcomas, glioblastoma (GBM), and melanoma (Fig. 1C; Table 1). Cancer cell lines derived from these mesenchymal tumor types often expressed LRRC15 protein at high levels *in vitro* (Supplementary Fig. S2A and S2B). To identify the type of stromal cell that expresses LRRC15 within tumors, double-staining assays were performed that revealed LRRC15 expression occurs on α-SMA+ CAFs in (Fig. 1D), and in other tumor types such as breast and pancreatic cancer.

Table 1. Summary of LRRC15 expression in cancer

	IHC score (TMA + individual tissues)	
Tumor type	**$\geq$ 2+**	**% Positive**
Breast		
Ductal + lobular	72/76	95
Triple-negative	10/11	91
Head and neck (incl. metastases)	182/226	81
Lung		
NSCLC: adeno	63/87	72
NSCLC: squamous	74/115	64
Pancreatic	27/41	66
Bladder	14/30	47
Colorectal	19/43	44
Ovarian	8/18	44
Hepatocellular	7/17	41
Testicular	9/31	29
Endometrial	3/27	11
Gastric	2/35	6
Renal	1/31	3
Gastrointestinal stromal tumor	0/6	0
Prostate	0/34	0
Sarcoma (multiple subtypes)[a]	28/39	72
Melanoma[a]	28/48	58
GBM[a]	7/31	23

NOTE: Biopsies from different tumor types were used to generate TMA, which were assessed for LRRC15 expression by IHC and scored on a scale of 0 to 4. A score of $\geq$2 was chosen to identify tumors (cancer cells or tumor stroma) that expressed LRRC15 at high levels. The LRRC15 staining and expression was only seen on the tumor stroma, unless otherwise stated.

Abbreviation: TMA, tissue microarrays.

[a]Indications where examples of cancer-positive LRRC15 expression were observed.

Normal tissue expression of LRRC15 and its regulation by TGFβ

Analysis of LRRC15 mRNA expression suggested its general absence from most normal human tissues (Fig. 1A; Supplementary Fig. S1), which was confirmed by a broad IHC assessment of LRRC15 protein expression (Fig. 2A). Interestingly, LRRC15 normal expression was highly localized with expression restricted to hair follicles, tonsil, stomach (cardia and pylorus regions only), spleen (peritrabecular region), osteoblasts, and sites of wound healing (Fig. 2A).

The recruitment and activation of fibroblasts in tumor stroma to become α-SMA-positive CAFs is known to be regulated in large part by the secretion of TGFβ in the TME (21–24). Given the expression of LRRC15 on CAFs, we decided to test whether LRRC15 expression was regulated by TGFβ. NHLFs, which express very low levels of LRRC15 *in vitro*, were found to upregulate LRRC15 expression upon treatment with TGFβ (10 ng/mL) by flow cytometry (Fig. 2B). NHLF cells that had sustained exposure to TGFβ for 7 days demonstrated that the induced LRRC15 expression was maintained, and these cells also showed an increase in expression of the intracellular CAF marker α-SMA (Fig. 2C). TGFβ-induced LRRC15 expression was found to be reversible upon removal of TGFβ from culture, and could also be inhibited by a TGFBR blocking antibody (Fig. 2D); further emphasizing the important role TGFβ plays in regulating LRRC15 expression.

LRRC15 is a novel marker of MSCs

The normal tissues that express LRRC15 are sites where TGFβ is reported to be present and where MSCs are known to reside (25–28). To test whether MSCs express LRRC15, BM-MSCs were acquired and tested for LRRC15 expression by flow cytometry and immunoblotting. BM-MSCs from several human donors showed significant LRRC15 expression when cultured *ex vivo*, and this expression was further increased upon treatment with TGFβ (Fig. 2E and F). In fact, LRRC15 expression and its induction by TGFβ were also seen in adipose-derived MSCs. A subset of umbilical cord–derived MSCs (ATCC) showed LRRC15 expression, albeit at lower levels than BM-MSCs or adipose MSCs

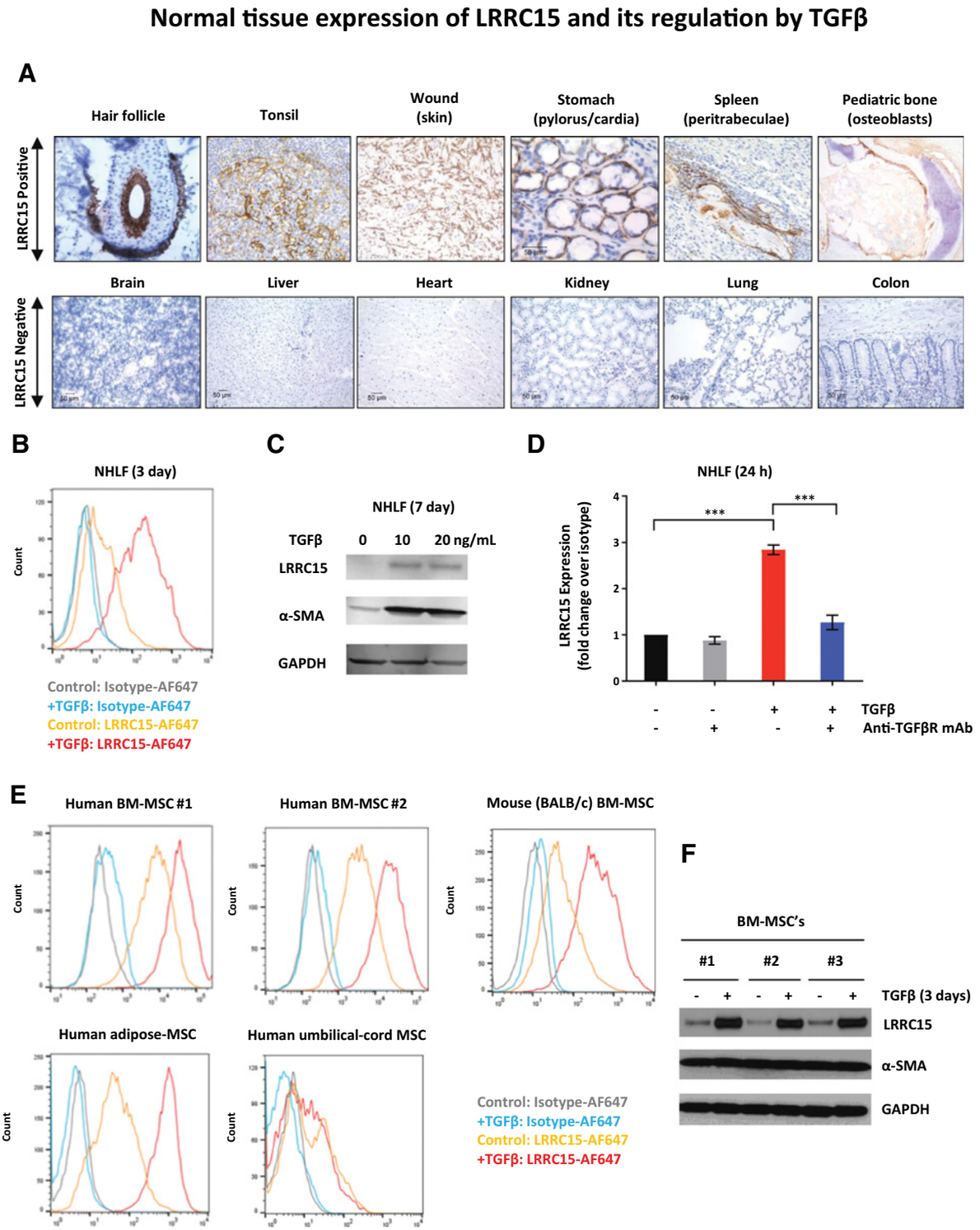

Figure 2.

Normal tissue expression of LRRC15 and its regulation by TGFβ. **A,** Representative IHC images of LRRC15-positive expression (top) and LRRC15-negative expression (bottom) in normal human tissues. **B,** Flow cytometry of LRRC15 expression on normal lung fibroblasts (NHLF) following stimulation with TGFβ (10 ng/mL). **C,** Immunoblot of LRRC15 and α-SMA expression in NHLF cell lysate following 7-day treatment with TGFβ (as indicated). **D,** LRRC15 induction by TGFβ in the presence and absence of a TGFBR-blocking antibody as measured by flow cytometry. **E,** Expression of LRRC15 on human MSCs (bone marrow, adipose, or umbilical derived) and mouse BM-MSCs treated with TGFβ (3 days). **F,** Immunoblots of LRRC15 and α-SMA expression for three distinct donor BM-MSCs with and without TGFβ treatment (3 days). Two-tailed *t* test (unequal variance). *, $P < 0.05$; **, $P < 0.01$; ***, $P < 0.001$.

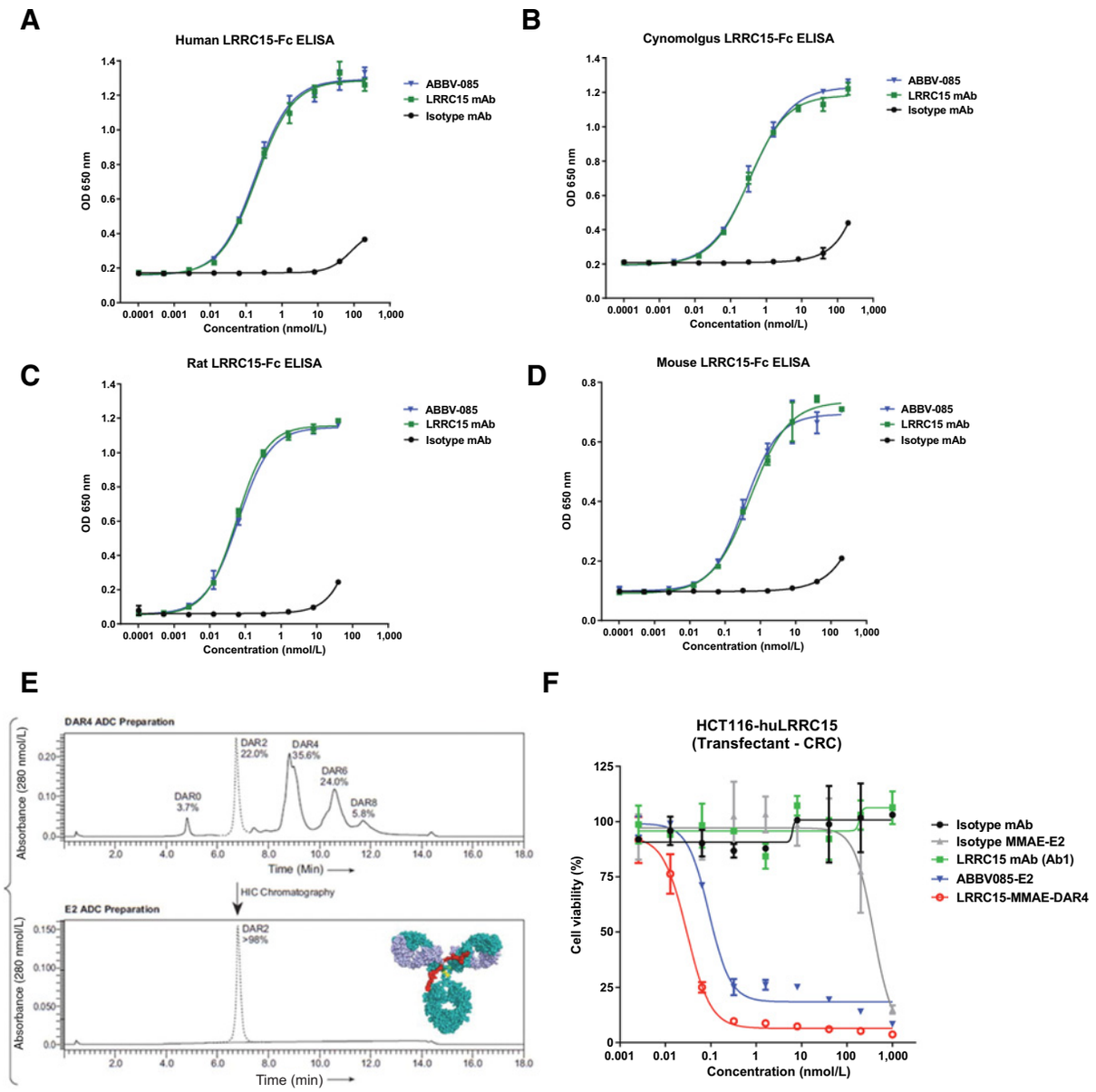

Figure 3.

In vitro characterization of the ADC ABBV-085. **A–D,** Binding by ELISA of isotype control antibody, LRRC15 antibody (Ab1), and ABBV-085 to human, cynomolgus monkey, rat, and mouse LRRC15-Fc recombinant protein. **E,** HIC of mc-vc-MMAE conjugated onto LRRC15 antibody (Ab1) via reduced interchain disulfides to a broad DAR4 distribution. ABBV-085 is shown containing primarily two mc-vcMMAE molecules per antibody (E2). **F,** Cell killing by LRRC15 antibody (Ab1) and ABBV-085 of HCT-116 cells stably expressing LRRC15 relative to isotype antibody and ADC controls.

(Fig. 2E). Mouse BM-MSCs (BALB/c strain) were similarly tested and confirmed to have LRRC15 expression, which was further increased following TGFβ treatment (Fig. 2E).

ABBV-085 is an LRRC15-targeting ADC with MMAE-driven bystander tumor efficacy

To assess if LRRC15 could be used as a targeting antigen to deliver a cytotoxic drug to the TME and elicit an antitumor response, an ADC was generated against the extracellular domain of LRRC15. The LRRC15-specific humanized IgG1 antibody (LRRC15 Ab1) has comparable protein binding across a broad range of species (human, cynomolgus monkey, rat, mouse) as shown by ELISA binding to LRRC15-Fc-fusion proteins and engineered LRRC15 transfectant cell lines containing the specific LRRC15 protein sequence for each species (Fig. 3A–D; Supplementary Table S1A). The parent LRRC15

antibody (Ab1) did not demonstrate *in vitro* or *in vivo* activity (as measured by direct inhibition of growth or by mediating ADCC; Supplementary Fig. S3A and S3B). ABBV-085 is a LRRC15-targeting antibody conjugated to the potent cell permeable antimitotic molecule MMAE through a cleavable vc dipeptide linker (29). Following conjugation to interchain disulfides, a process step is added to highly enrich for ADC molecules containing primarily two MMAE molecules per antibody (ADCs with this conjugation format are referred to as "E2" throughout). This differs from the more commonly used drug–antibody ratio (DAR) with a Gaussian distribution averaging ∼4 (DAR4; Fig. 3E), such as that used in the approved agent brentuximab vedotin. The drug-loading profile of two MMAE molecules (E2) was chosen over DAR4 based on the combination of preclinical efficacy (Supplementary Fig. S4A) and significantly improved tolerability in toxicity models (e.g., rat tolerability; Supplementary Table S1B). ABBV-085 is able to kill LRRC15 expressing cancer cells *in vitro* (Fig. 3F), and because ABBV-085 can bind to mouse LRRC15, its efficacy was assessed in xenograft models where the implanted human cancer cells were either LRRC15-positive or -negative, and the mouse stromal fibroblasts were LRRC15-positive. We found that ABBV-085 has broad efficacy (tumor regressions or cures) *in vivo* in many solid tumor models across multiple cancer indications. Efficacy was observed in LRRC15 stromal fibroblast-positive/cancer-negative models, and in LRRC15 cancer-positive models. As examples, the NCI-H1650 (NSCLC-adenocarcinoma) model, which was cancer-negative but highly positive for mouse stromal LRRC15 expression (3+ IHC), displayed robust LRRC15-targeted sensitivity to ABBV-085, including tumor regressions and cures (>80 days postinitiation of treatment), which was superior to the treatment with carboplatin or erlotinib (Fig. 4A). In addition, ABBV-085 demonstrated significant antitumor activity in multiple LRRC15 cancer-positive models, including a PDX model of osteosarcoma (CTG-0241) with high LRRC15 cancer and stromal expression (3+ IHC). This PDX model was refractory to current therapies used in osteosarcoma when dosed maximally (doxorubicin, ifosfamide, gemcitabine, cisplatin; Fig. 4B). Of note, tumors that eventually regrew following ABBV-085 treatment, retained sensitivity to ABBV-085 when the ADC was re-administered in both the LRRC15 cancer-negative/stromal-positive setting (SUM190PT breast xenografts; Fig. 4C) and in LRRC15 cancer-positive/stromal-positive tumors (U118MG GBM xenografts; Fig. 4D).

ABBV-085 also showed enhanced activity in combination with multiple therapies of varying mechanisms of action (Fig. 5A–D; Supplementary Fig. S4B and S4C), which was statistically superior to either agent alone, including cytotoxic chemotherapy (gemcitabine, docetaxel), radiation, immune-therapy (anti-PD1), and other targeted therapies (erlotinib, cetuximab). The broad combination activity with ABBV-085 frequently resulted in CRs and cures in these xenograft models (both cell line and patient-derived). All mice tolerated ABBV-085 in combination with the agents tested, indicating no worsening of tolerability associated with these combinations.

To further our understanding of ABBV-085 mechanism of action, we assessed its ability to induce M-phase cell-cycle arrest via uptake of the mitotic inhibitor MMAE. M-phase cell-cycle arrest (by DNA flow cytometry) was demonstrated in LRRC15-positive U118-MG cancer cells *in vitro* (Supplementary Fig. S5A). To assess ABBV-085 mechanism of killing of LRRC15-negative cancer cells *in vivo*, EBC-1 tumors (cancer-negative, LRRC15 stroma-positive) were excised 72 hours posttreatment, and stained by IHC for phospho-histone-H3 (pHH3), a marker of cells in mitosis. The LRRC15-negative cancer cells underwent a transient M-phase mitotic arrest, as noted by an increase in pHH3 staining (Fig. 6A). This suggested that the payload was exerting a targeted bystander activity on the cancer cells following its initial uptake and processing by the LRRC15-positive stromal fibroblasts. To assess this further, a non-cell-permeable, yet structurally similar, highly potent antimitotic payload monomethyl auristatin-F (MMAF) was conjugated onto the LRRC15 Ab1 and evaluated (30). *In vitro*, the LRRC15-MMAF ADC was able to kill LRRC15-positive cancer cells at subnanomolar potency, similar to that seen for ABBV-085 (Supplementary Fig. S5B). *In vivo*, however, the MMAF payload proved to be ineffective in LRRC15 cancer-negative/stromal-positive xenograft models (PANC1, EBC1) shown to be sensitive to ABBV-085 (Fig. 6B and C). This suggests that direct killing of the LRRC15-positive CAFs by ABBV-085 only partially contributes to tumor reduction and that the cell permeable properties of MMAE are essential to ABBV-085's *in vivo* activity. To investigate the mechanism of ABBV-085 further, EBC-1 tumors were excised at Day 11 posttreatment, dispersed into single cell suspensions and evaluated by flow cytometry or immunofluorescent microscopy. We found that ABBV-085 resulted in a significant reduction in the percentage of cancer cells (EpCAM-positive) within the shrinking tumor (Fig. 6D and E). Interestingly, our *ex vivo* data of dispersed tumors revealed that LRRC15-positive fibroblasts were not completely ablated by ABBV-085 treatment in shrinking tumors (e.g., EBC1, PANC1). A population of α-SMA- and FAPα-positive fibroblasts were still evident post treatment (by microscopy and flow cytometry, respectively), suggesting that ABBV-085 was having a more pronounced growth-inhibitory effect on the cancer cells than on the stromal fibroblasts in our models (Fig. 6D and E; Supplementary Fig. S6). A significant increase in mouse macrophages ($F4/80^+$) was also seen within the shrinking tumor post-ABBV-085 treatment (Fig. 6E). These observations, together with the immunogenic cell death (ICD) reported for other MMAE ADCs preclinically and clinically, suggest that additional investigation of a possible immune-modulating aspect to ABBV-085 is warranted (31, 32).

To further examine the potential impact of bystander killing by the MMAE payload, an assessment of the proliferative rate (Ki67 positivity) of cancer cells versus stromal cells was performed by immunohistochemistry on multiple human solid tumor tissue types (Fig. 6F). Across tumor indications, the stromal fibroblast compartment had a much lower percentage of Ki67+ proliferative cells than was seen for the corresponding cancer area within each tumor type.

Discussion

Herein, we performed the first detailed assessment of LRRC15 expression in tumor and normal tissues. We found this novel protein to be highly expressed on CAFs within the tumor stroma of many cancer indications, as well as directly on cancer cells from a subset of mesenchymal tumors (e.g., sarcomas, GBM). Consistent with the mesenchymal cancer expression, we found LRRC15 to be expressed on localized normal tissues with mesenchymal

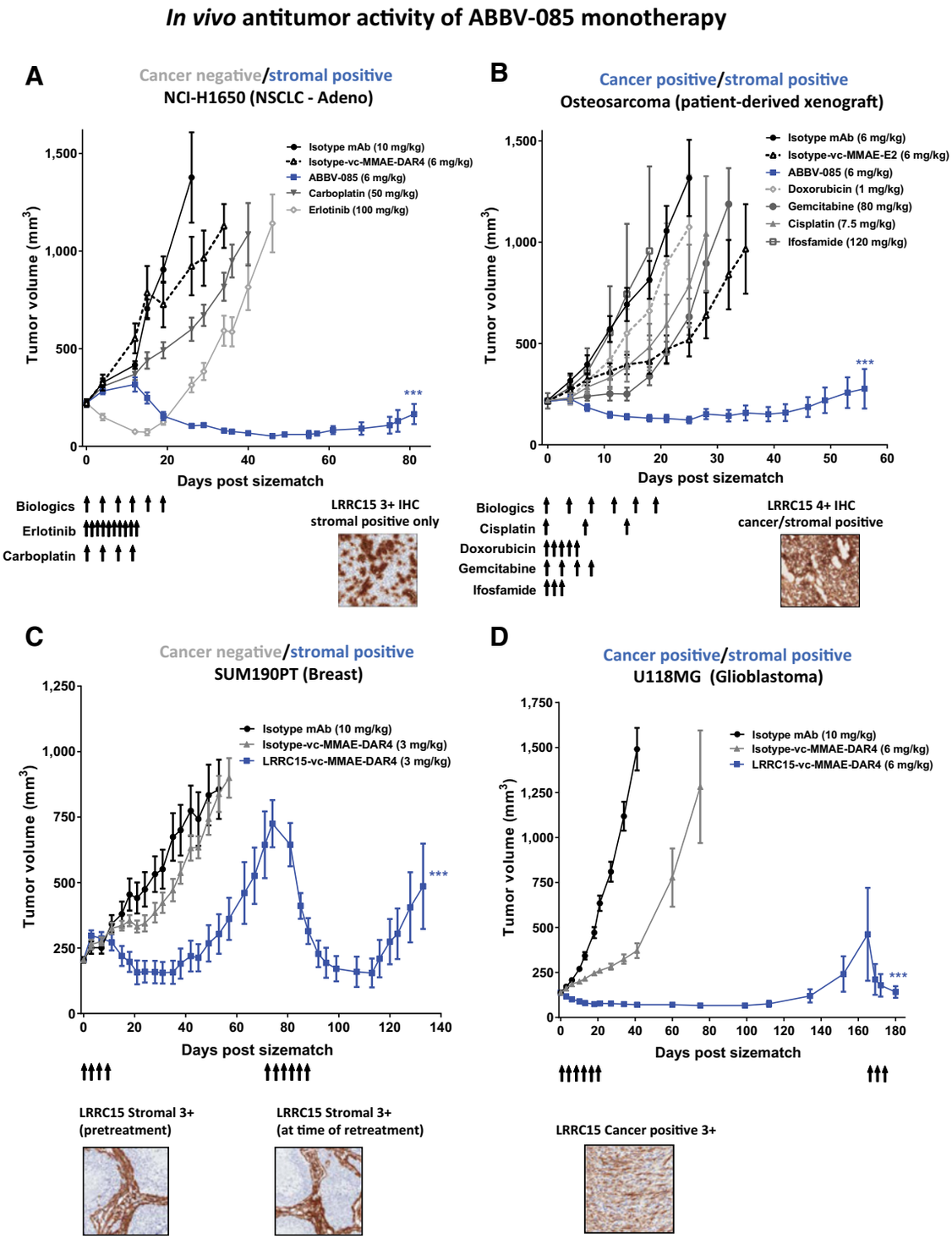

Figure 4.

In vivo antitumor activity of ABBV-085 monotherapy. **A,** Tumor growth curves for NCI-H1650 xenografts (LRRC15 cancer-negative/stromal-positive) treated with ABBV-085, carboplatin, or erlotinib as indicated. **B,** Tumor growth curves for osteosarcoma PDX CTG-0241 (LRRC15 cancer-positive/stromal-positive) treated with ABBV-085 and compared with the listed chemotherapy agents at their respective maximal dose/schedule. **C** and **D,** Retreatment of xenograft models that eventually regrew post-initial ADC treatment and response. Mice were retreated with anti-LRRC15-vcMMAE as indicated with LRRC15-ADC for cancer-negative/stromal-positive tumors (SUM190PT, breast) and cancer-positive/stromal-positive tumors (U118MG, GBM). Tumor growth studies are dosed as indicated and are depicted as mean ± SEM. *, $P < 0.05$; **, $P < 0.01$; ***, $P < 0.001$ by two-way ANOVA with *post hoc* Bonferroni correction.

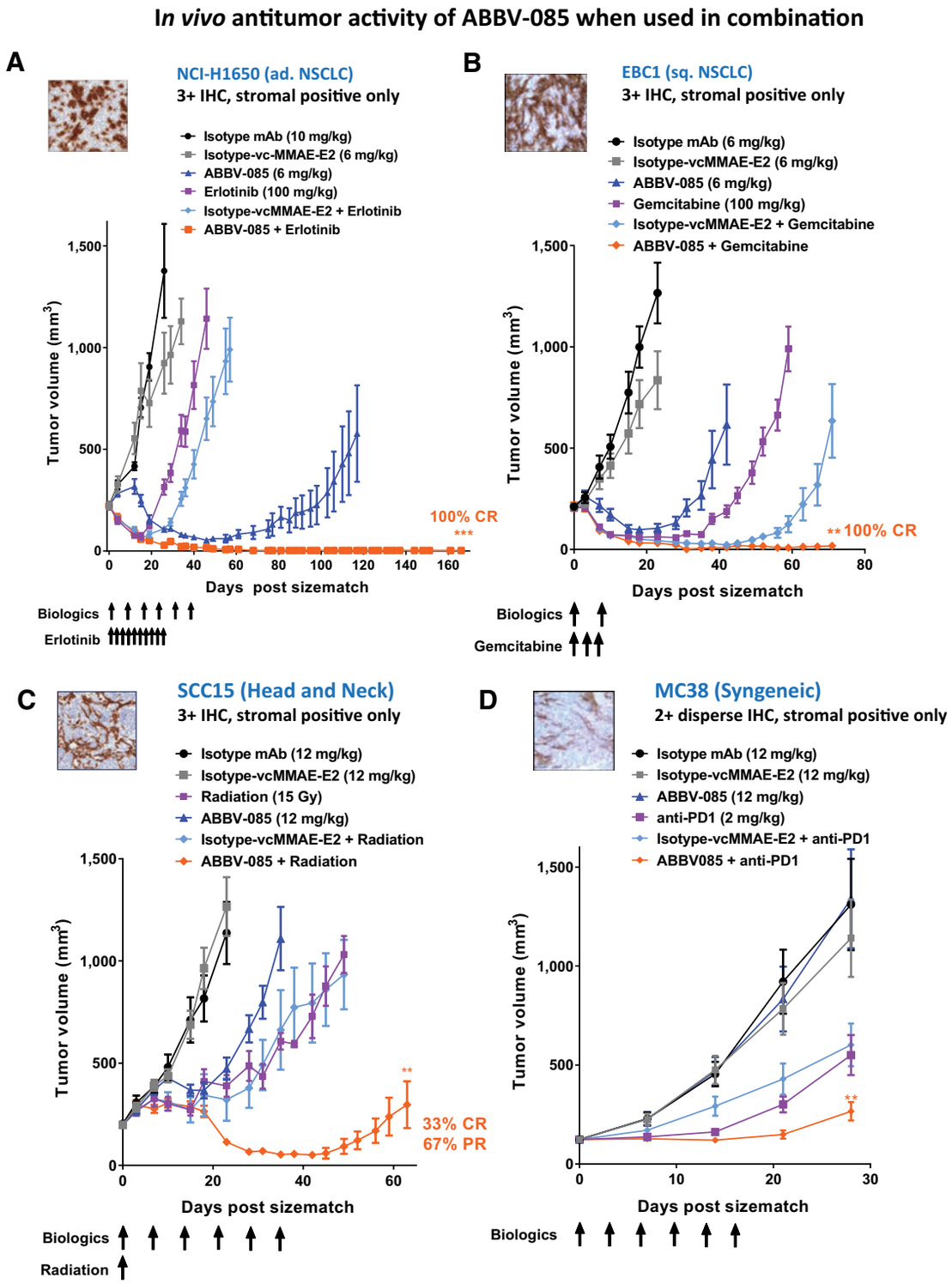

Figure 5.

In vivo antitumor activity of ABBV-085 when used in combination with anticancer drugs. Tumor growth curves of ABBV-085 combined with erlotinib in NSCLC-adeno model NCI-H1650 (**A**) and gemcitabine in squamous lung xenograft model EBC-1 (**B**). **C,** Radiation in the head and neck xenograft model SCC15. Xenograft models tested were LRRC15 cancer-negative/stromal-positive. **D,** Anti-PD1 in MC38 syngeneic model (LRRC15 cancer-negative/weakly stromal-positive). Tumor growth studies are dosed as indicated and are depicted as mean ± SEM. *, $P < 0.05$; **, $P < 0.01$; ***, $P < 0.001$ by two-way ANOVA with *post hoc* Bonferroni correction.

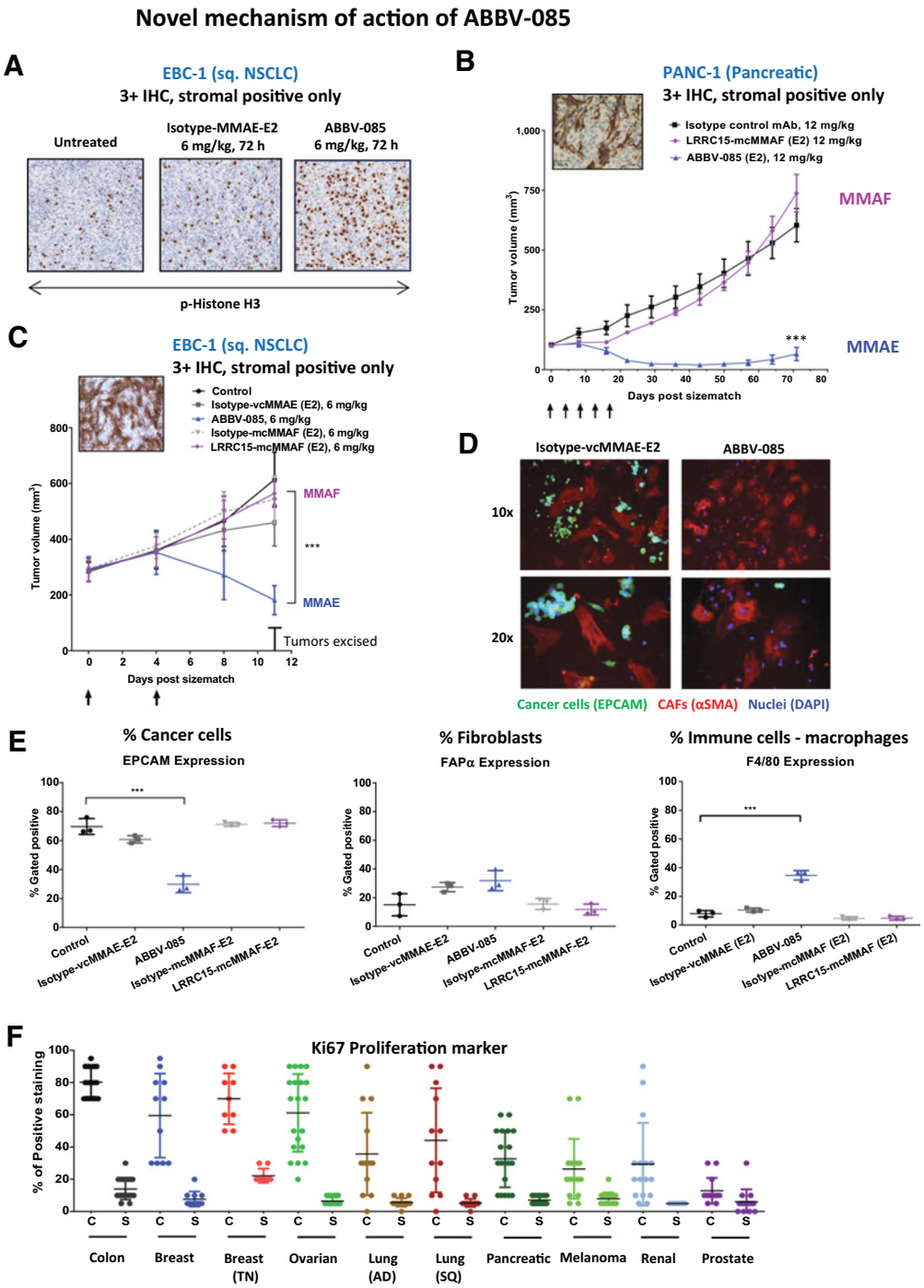

Figure 6.

Mechanism of ABBV-085. **A,** Representative IHC analysis showing phospho-histone-H3 (M-phase mitotic arrest) in EBC-1 (LRRC15 cancer-negative/stromal-positive) xenografts treated with ABBV-085 or isotype controls and harvested 72 hours after dosing. **B,** PANC-1 (LRRC15 cancer-negative/stromal-positive) xenograft tumors showing sensitivity to anti-LRRC15-vcMMAE (ABBV-085) but not anti-LRRC15-mcMMAF. **C,** EBC-1 xenograft tumors treated with ABBV-085, LRRC15-mcMMAF, or isotype ADCs, which were subsequently harvested for *ex vivo* analysis on day 11. **D,** Representative fluorescent microscopy of EBC-1–dispersed tumors (day 11, as indicated in **C**) allowed to adhere to slides (24 hours) and imaged for cancer cells (EPCAM, green), CAFs (α-SMA, red), and nuclei (DAPI, blue). **E,** Flow cytometry of EBC-1–treated tumors harvested 11 days posttreatment and dispersed into single cells. The relative percentage of human cancer cells (EPCAM), mouse fibroblasts (FAPα), or mouse immune cells (F4/80$^+$ macrophages) was determined and compared across groups. **F,** IHC analysis of percent Ki67-positive staining (proliferation marker) of cancer versus stromal compartments within tumor surgical samples across different solid tumor indications, as assessed by hematoxylin and eosin staining and pathology review. C, cancer cells; S, stromal cells; TN, triple-negative; AD, adeno; SQ, squamous.

characteristics such as hair follicle and tonsil (25, 26). The expression of LRRC15 observed on both CAFs and MSCs, as well as on wound healing tissue (all of which are highly TGFβ-regulated), supports the theory that similar cell populations and processes are at play in tumor stroma and wound repair (33, 34).

Based on our expression findings, we propose that LRRC15 is a novel cell-surface marker of the mesenchymal phenotype, with high expression limited to activated fibroblasts, MSCs, and a subset of mesenchymal cancer cells (35). The specific localization of LRRC15 protein expression and its inducibility by TGFβ differentiates LRRC15 from other commonly used mesenchymal markers such as FAPα, which have expression on cells other than myofibroblasts (36, 37). This is further supported by RNA-seq expression data from TCGA breast cancer cohorts (https://cancergenome.nih.gov/), where we observed lower baseline LRRC15 normal tissue expression and higher differential LRRC15 RNA expression between cancer and adjacent normal tissues, compared with that seen for FAPα (Supplementary Fig. S7).

Because the role of CAFs as regulators of tumor growth is the subject of ongoing debate (especially across tumor types), attempts at modulating this cell population need to be carefully considered (12, 38, 39). Our data on LRRC15 expression suggest that the heterogeneity of CAFs, due to its cell type of origin, may be a contributor to these discrepancies. Because LRRC15 is a cell surface marker with specific expression on CAFs (including recruited MSCs and TGFβ-activated fibroblasts), with limited expression on normal cells, we believe it to be a valuable antigen that can be leveraged both in the study of the TME, and for the delivery of cytotoxic agents. Given the scarcity of published data on this novel protein, additional work is needed to better understand the biological and functional role of LRRC15 within the TME.

The clinical failure of smoothened inhibitors that targeted CAFs in pancreatic cancer and resulted in increased tumor growth emphasizes the need for an increased understanding of distinct stromal cell populations and their specific roles in regulating cell growth in different cancer indications (40, 41). These smoothened inhibitors targeted CAFs without also negatively impacting the growth of cancer cells, suggesting a treatment strategy in pancreatic cancer (and possibly other indications) that only depletes CAFs while having no inhibitory effect on cancer cells is unlikely to demonstrate positive clinical activity (42).

ABBV-085 uses an LRRC15-specific mAb to localize the MMAE payload at high levels in the TME. Once localized to the LRRC15-rich stroma, the cell-permeable MMAE payload can diffuse into nearby cancer cells where it can then drive a targeted-bystander effect to kill dividing cancer cells and ultimately induce tumor shrinkage. We found ABBV-085 to have a more profound growth inhibitory effect on proliferative cancer cells within a tumor than the stromal fibroblasts, which tend to have a lower Ki67 mitotic rate (Fig. 6D–F). Similarly, LRRC15-positive MSCs, which also have a low proliferative rate, displayed minimal sensitivity to ABBV-085 *in vitro*, alleviating potential normal tissue toxicity concerns of targeting these MSCs. In both rat (Supplementary Table S1B) and cynomolgus monkey tolerability studies for ABBV-085, no toxicities associated with sites of normal tissue LRRC15 expression were observed. Rather the dose limiting toxicity was neutropenia, which is a well characterized and frequently observed finding with other MMAE-based ADCs (43, 44).

ABBV-085 monotherapy activity was seen in both LRRC15 cancer-negative/stromal-positive tumor models and in LRRC15 cancer-positive/stromal-positive tumors. In addition, ABBV-085 displayed activity in highly chemo-refractive indications such as osteosarcoma (CTG-0241 PDX; Fig. 4B) with poor treatment options and prognosis (45). Xenograft models across multiple solid tumor indications (e.g., breast, lung, head and neck, pancreatic, sarcoma, GBM) with $\geq$2+ LRRC15 positivity (25% area, moderate/strong staining) often responded to ABBV-085 treatment, suggesting that tumors with high LRRC15 positivity are more likely to respond and that ABBV-085 has the potential to be broadly active. Interestingly, we found that tumors that eventually regrow following ABBV-085 treatment retain sensitivity to ABBV-085 upon re-administration of the ADC (Fig. 4C and D). We propose that targeting an antigen found on CAFs, which are under less genetic/mutation pressure compared with cancer cells may minimize potential drug resistance due to reduced target antigen expression.

Encouraging antitumor efficacy is also seen when ABBV-085 is used in combination with multiple cancer therapies with varying mechanisms of action (Fig. 5A–D; Supplementary Fig. S4B and S4C). We propose that targeting the LRRC15-positive TME using ABBV-085 has the potential to enhance the delivery and activity of these combination therapeutic agents, resulting in improved anticancer activity relative to that seen for either single agent alone. It will need to be determined clinically whether high LRRC15 cancer-positive/stromal-positive indications (e.g., sarcoma) or high expressing LRRC15 cancer-negative-/stromal-positive indications (e.g., breast, head, and neck) respond better to ABBV-085 treatment and whether the appropriate clinical development is as a monotherapy or in the combination setting.

A companion diagnostic IHC assay (CDx) has been created to support the clinical development of ABBV-085. Patient selection for LRRC15 expression may be required in certain cancer indications where the prevalence of antigen positivity is lower. A retrospective assessment of LRRC15 expression and its potential correlation with clinical response will also be determined.

In summary, LRRC15 is a novel marker of TGFβ-activated fibroblasts and MSCs and can be used as a targeting antigen to deliver an ADC payload to the TME. ABBV-085 is a first-in-class stromal targeting ADC that is currently being investigated in a phase I safety study in solid tumors expressing LRRC15.

Disclosure of Potential Conflicts of Interest

J.W. Purcell has ownership interest (including patents) in AbbVie. S.E. Morgan-Lappe has ownership interest (including patents) in AbbVie. E.D. Hsi reports receiving other commercial research support from Abbvie. No potential conflicts of interest were disclosed by the other authors.

Authors' Contributions

Conception and design: J.W. Purcell, S.G. Tanlimco, T. Uziel, R. Powers, J. Samayoa, J.P. Palma, K. Gish, S.E. Morgan-Lappe, D.T. Chao

Development of methodology: J.W. Purcell, S.G. Tanlimco, J. Hickson, M. Sho, R. Powers, T. McGonigal, S. Kumar, J. Samayoa, D. Zhang, S. Mishra, E.D. Hsi

Acquisition of data (provided animals, acquired and managed patients, provided facilities, etc.): J.W. Purcell, S.G. Tanlimco, J. Hickson, M. Fox, M. Sho, L. Durkin, T. Uziel, R. Powers, K. Foster, T. McGonigal, S. Kumar, J. Samayoa, D. Zhang, S. Mishra, E.D. Hsi

Analysis and interpretation of data (e.g., statistical analysis, biostatistics, computational analysis): J.W. Purcell, S.G. Tanlimco, J. Hickson, M. Sho, T. Uziel, T. McGonigal, S. Kumar, J. Samayoa, D. Zhang, J.P. Palma, S. Mishra, E.D. Hsi, D.T. Chao

Writing, review, and/or revision of the manuscript: J.W. Purcell, S.G. Tanlimco, J. Hickson, T. Uziel, J. Samayoa, D. Zhang, D. Hollenbaugh, K. Gish, S.E. Morgan-Lappe, E.D. Hsi, D.T. Chao

Administrative, technical, or material support (i.e., reporting or organizing data, constructing databases): D. Zhang
Study supervision: J.W. Purcell, J. Hickson, K. Gish, D.T. Chao
Other (contributions to design/evaluation of preclinical in vivo studies by IHC): J.P. Palma

Acknowledgments

We thank Dr. Thomas Hudson and Dr. Francesco Marincola for advice with the manuscript preparation. And the following contributors to data contained within the manuscript: Daniel Serna (ADCC assays), Bob Duffy (HIC), Lise Loberg (rat tolerability), Jerry Clarin (IHC).

The costs of publication of this article were defrayed in part by the payment of page charges. This article must therefore be hereby marked *advertisement* in accordance with 18 U.S.C. Section 1734 solely to indicate this fact.

Received January 30, 2018; revised March 26, 2018; accepted May 10, 2018; published first May 15, 2018.

References

1. Erkan M, Hausmann S, Michalski CW, Fingerle AA, Dobritz M, Kleeff J, et al. The role of stroma in pancreatic cancer: diagnostic and therapeutic implications. Nat Rev Gastroenterol Hepatol 2012;9:454–67.
2. Giacchetti S, Porcher R, Lehmann-Che J, Hamy AS, de Roquancourt A, Cuvier C, et al. Long-term survival of advanced triple-negative breast cancers with a dose-intense cyclophosphamide/anthracycline neoadjuvant regimen. Br J Cancer 2014;110:1413–9.
3. Gajra A, Jatoi A. Non-small-cell lung cancer in elderly patients: a discussion of treatment options. J Clin Oncol 2014;32:2562–9.
4. Turley SJ, Cremasco V, Astarita JL. Immunological hallmarks of stromal cells in the tumour microenvironment. Nat Rev Immunol 2015;15:669–82.
5. Feig C, Gopinathan A, Neesse A, Chan DS, Cook N, Tuveson DA. The pancreas cancer microenvironment. Clin Cancer Res 2012;18:4266–76.
6. Olive KP, Jacobetz MA, Davidson CJ, Gopinathan A, McIntyre D, Honess D, et al. Inhibition of Hedgehog signaling enhances delivery of chemotherapy in a mouse model of pancreatic cancer. Science 2009;324:1457–61.
7. Berchtold S, Grunwald B, Kruger A, Reithmeier A, Hahl T, Cheng T, et al. Collagen type V promotes the malignant phenotype of pancreatic ductal adenocarcinoma. Cancer Lett 2015;356:721–32.
8. Jones SF, Siu LL, Bendell JC, Cleary JM, Razak AR, Infante JR, et al. A phase I study of VS-6063, a second-generation focal adhesion kinase inhibitor, in patients with advanced solid tumors. Invest New Drugs 2015;33:1100–7.
9. Hingorani SR, Harris WP, Beck JT, Berdov BA, Wagner SA, Pshevlotsky EM, et al. Phase Ib study of PEGylated recombinant human hyaluronidase and gemcitabine in patients with advanced pancreatic cancer. Clin Cancer Res 2016;22:2848–54.
10. Jiang H, Hegde S, Knolhoff BL, Zhu Y, Herndon JM, Meyer MA, et al. Targeting focal adhesion kinase renders pancreatic cancers responsive to checkpoint immunotherapy. Nat Med 2016;22:851–60.
11. Madar S, Goldstein I, Rotter V. `Cancer associated fibroblasts'–more than meets the eye. Trends Mol Med 2013;19:447–53.
12. Kalluri R. The biology and function of fibroblasts in cancer. Nat Rev Cancer 2016;16:582–98.
13. Buchsbaum RJ, Oh SY. Breast cancer-associated fibroblasts: where we are and where we need to go. Cancers (Basel) 2016;8. doi: 10.3390/cancers8020019.
14. Shiga K, Hara M, Nagasaki T, Sato T, Takahashi H, Takeyama H. Cancer-associated fibroblasts: their characteristics and their roles in tumor growth. Cancers (Basel) 2015;7:2443–58.
15. Augsten M. Cancer-associated fibroblasts as another polarized cell type of the tumor microenvironment. Front Oncol 2014;4:62. doi: 10.3389/fonc.2014.00062.
16. Lambert JM, Morris CQ. Antibody-drug conjugates (ADCs) for personalized treatment of solid tumors: a review. Adv Ther 2017;34:1015–35.
17. Diamantis N, Banerji U. Antibody-drug conjugates—an emerging class of cancer treatment. Br J Cancer 2016;114:362–7.
18. McDonagh CF, Turcott E, Westendorf L, Webster JB, Alley SC, Kim K, et al. Engineered antibody-drug conjugates with defined sites and stoichiometries of drug attachment. Protein Eng Des Sel 2006;19:299–307.
19. Satoh K, Hata M, Yokota H. High lib mRNA expression in breast carcinomas. DNA Res 2004;11:199–203.
20. Schuetz CS, Bonin M, Clare SE, Nieselt K, Sotlar K, Walter M, et al. Progression-specific genes identified by expression profiling of matched ductal carcinomas in situ and invasive breast tumors, combining laser capture microdissection and oligonucleotide microarray analysis. Cancer Res 2006;66:5278–86.
21. Kalluri R, Zeisberg M. Fibroblasts in cancer. Nat Rev Cancer 2006;6:392–401.
22. Ronnov-Jessen L, Petersen OW. Induction of alpha-smooth muscle actin by transforming growth factor-beta 1 in quiescent human breast gland fibroblasts. Implications for myofibroblast generation in breast neoplasia. Lab Invest 1993;68:696–707.
23. Lohr M, Schmidt C, Ringel J, Kluth M, Muller P, Nizze H, et al. Transforming growth factor-beta1 induces desmoplasia in an experimental model of human pancreatic carcinoma. Cancer Res 2001;61:550–5.
24. Pickup M, Novitskiy S, Moses HL. The roles of TGFbeta in the tumour microenvironment. Nat Rev Cancer 2013;13:788–99.
25. Wang Y, Liu J, Tan X, Li G, Gao Y, Liu X, et al. Induced pluripotent stem cells from human hair follicle mesenchymal stem cells. Stem Cell Rev 2013;9:451–60.
26. Lee BJ, Kang DW, Park HY, Song JS, Kim JM, Jang JY, et al. Isolation and localization of mesenchymal stem cells in human palatine tonsil by W5C5 (SUSD2). Cell Physiol Biochem 2016;38:83–93.
27. Heino TJ, Hentunen TA. Differentiation of osteoblasts and osteocytes from mesenchymal stem cells. Curr Stem Cell Res Ther 2008;3:131–45.
28. Maxson S, Lopez EA, Yoo D, Danilkovitch-Miagkova A, Leroux MA. Concise review: role of mesenchymal stem cells in wound repair. Stem Cells Transl Med 2012;1:142–9.
29. Jain N, Smith SW, Ghone S, Tomczuk B. Current ADC linker chemistry. Pharm Res 2015;32:3526–40.
30. Li F, Emmerton KK, Jonas M, Zhang X, Miyamoto JB, Setter JR, et al. Intracellular released payload influences potency and bystander-killing effects of antibody-drug conjugates in preclinical models. Cancer Res 2016;76:2710–9.
31. Herrera AF, Moskowitz AJ, Bartlett NL, Vose JM, Ramchandren R, Feldman TA, et al. Interim results of brentuximab vedotin in combination with nivolumab in patients with relapsed or refractory Hodgkin lymphoma. Blood 2018;131:1183–94.
32. Muller P, Martin K, Theurich S, Schreiner J, Savic S, Terszowski G, et al. Microtubule-depolymerizing agents used in antibody-drug conjugates induce antitumor immunity by stimulation of dendritic cells. Cancer Immunol Res 2014;2:741–55.
33. Dvorak HF. Tumors: wounds that do not heal. Similarities between tumor stroma generation and wound healing. N Engl J Med 1986;315:1650–9.
34. Ohlund D, Elyada E, Tuveson D. Fibroblast heterogeneity in the cancer wound. J Exp Med 2014;211:1503–23.
35. Ye X, Weinberg RA. Epithelial-mesenchymal plasticity: a central regulator of cancer progression. Trends Cell Biol 2015;25:675–86.
36. Tchou J, Zhang PJ, Bi Y, Satija C, Marjumdar R, Stephen TL, et al. Fibroblast activation protein expression by stromal cells and tumor-associated macrophages in human breast cancer. Hum Pathol 2013;44:2549–57.
37. Reilkoff RA, Bucala R, Herzog EL. Fibrocytes: emerging effector cells in chronic inflammation. Nat Rev Immunol 2011;11:427–35.
38. Ozdemir BC, Pentcheva-Hoang T, Carstens JL, Zheng X, Wu CC, Simpson TR, et al. Depletion of carcinoma-associated fibroblasts and fibrosis induces immunosuppression and accelerates pancreas cancer with reduced survival. Cancer Cell 2014;25:719–34.
39. Pesic M, Greten FR. Inflammation and cancer: tissue regeneration gone awry. Curr Opin Cell Biol 2016;43:55–61.
40. Gu D, Schlotman KE, Xie J. Deciphering the role of hedgehog signaling in pancreatic cancer. J Biomed Res 2016;30:353–60.
41. Catenacci DV, Junttila MR, Karrison T, Bahary N, Horiba MN, Nattam SR, et al. Randomized phase Ib/II study of gemcitabine plus placebo or vismodegib, a Hedgehog pathway inhibitor, in patients with metastatic pancreatic cancer. J Clin Oncol 2015;33:4284–92.

42. Rhim AD, Oberstein PE, Thomas DH, Mirek ET, Palermo CF, Sastra SA, et al. Stromal elements act to restrain, rather than support, pancreatic ductal adenocarcinoma. Cancer Cell 2014;25:735–47.
43. Younes A, Gopal AK, Smith SE, Ansell SM, Rosenblatt JD, Savage KJ, et al. Results of a pivotal phase II study of brentuximab vedotin for patients with relapsed or refractory Hodgkin's lymphoma. J Clin Oncol 2012;30:2183–9.
44. Palanca-Wessels MC, Czuczman M, Salles G, Assouline S, Sehn LH, Flinn I, et al. Safety and activity of the anti-CD79B antibody-drug conjugate polatuzumab vedotin in relapsed or refractory B-cell non-Hodgkin lymphoma and chronic lymphocytic leukaemia: a phase 1 study. Lancet Oncol 2015;16:704–15.
45. Durfee RA, Mohammed M, Luu HH. Review of osteosarcoma and current management. Rheumatol Ther 2016;3:221–43.